An Integrated Capacitive Power Transfer System for Field Excitation of Wound Field Synchronous Machine

An Integrated Capacitive Power Transfer System for Field Excitation of Wound Field Synchronous Machine

Stefano Savio
Politecnico di Torino
Energy department "G. Ferraris"
Turin, Italy
stefano.savio@polito.it

Syed Muhammad Hassan Gillani, Ujjwal Pratik
Ritvik Chattopadhyay, Iqbal Husain, and Zeljko Pantic*
Department of Electrical and Computer Engineering
North Carolina State University
Raleigh, North Carolina
*zpantic@ncsu.edu

***Abstract*—The development of cost-effective electric vehicles has renewed interest in Wound Field Synchronous Machines (WFSMs) for traction applications. However, low efficiency and frequent maintenance of the brushes prevent a wider adoption of WFSMs. To overcome these challenges, the application of wireless power transfer systems for field excitation has recently been explored. This paper presents an integrated Capacitive Power Transfer (CPT) system for field excitation of WFSMs. The proposed coupling structure for CPT is placed within the air gap of the machine. The CPT coupling plates are made of magnetic material. The novelty of the proposed approach is that the presented design allows power transfer to the rotor without increasing the active volume of the machine. A preliminary feasibility analysis of the system is performed through Finite Element Analysis (FEA) simulations. A prototype with a stator and a Computer Numerical Control (CNC) fabricated replica of a rotor is developed to test the proposed CPT system. Experimental verification of the proposed power transfer system demonstrates an efficiency of 81.3% with a transferred power of 64 W at 2 MHz frequency.**

***Index Terms*—Capacitive Power Transfer (CPT), brushless, wireless power transfer, Wound Field Synchronous Machine (WFSM)**

I. Introduction

Interior Permanent Magnet (IPM) motors are widely used as traction motors due to their high-power density [1]. However, the inclusion of rare-earth PM materials results in a significant increase in the overall machine cost [2]. Contrary to IPM, WFSM utilizes DC power for rotor field excitation. The constant current supply to a rotating shaft is coupled with the requirement of brushes and slip rings. These brushes and slip rings establish a constant physical contact between the rotor and external DC source. Although being cost effective, they pose a challenge in terms of reduced efficiency and high maintenance [3]. These challenges have motivated the researcher to develop the field excitation system with higher efficiency and reduced maintenance [4]. An alternative way to avoid the use of brushes is the employment of an additional exciter rotor or rotary transformer [5], [6]. However, this increases the length of the machine significantly.

Wireless Power Transfer (WPT) techniques have heralded a compact and efficient design for field excitation. WPT is a convenient way to transmit power to a field winding. Inductive Power Transfer (IPT) eliminates the requirement of brushes but introduces ferrite material and Litz wire, which increases the mass and lowers the system efficiency [7]. Contrary to IPT, a CPT system employs low-cost and lightweight metal plates as capacitive couplers [8]. In general, CPT is more efficient for small gap applications ($\approx$1 mm) than IPT [9]. Moreover, if employed for field excitation, it does not require maintenance compared to traditional methods. In [10], a Printed Circuit Board (PCB) based CPT system has been implemented on the rotor shaft for excitation. However, this approach adds to the machine's active volume, thus reducing the power density.

This paper proposes a novel implementation of the CPT system. CPT coupler plates made of electrical steel are mounted on the rotor and stator across the air gap. This enables the excitation of the rotor without increasing the active length of the machine. The use of electrical steel maintains the effective air gap of the machine. Furthermore, it is demonstrated that the rotor and the stator act as shielding plates to prevent the stray electric field in the surrounding environment [11]. A research study on the feasibility of the proposed system is performed on a 36 slot/6 pole WFSM using FEA analysis. A prototype with a stator and a Computer Numerical Control (CNC) fabricated replica of a rotor is developed to test the proposed CPT system.

The organization of the manuscript is as follow: in Section II, design and modeling of the proposed CPT system is described. In Section III, modeling of WFSM in FEA is explained. In section IV, optimization based on FEA analysis and Pareto front is presented. Section V presents the experimental prototype development and testing. Section VI summarizes the main achievement of the study.

II. Design and Modeling of the Proposed Coupling Structure

The exploded view of the proposed design is shown in Fig. 1(a). A common six-plate coupling structure provides the basis for the coupler design. As mentioned, the novelty of

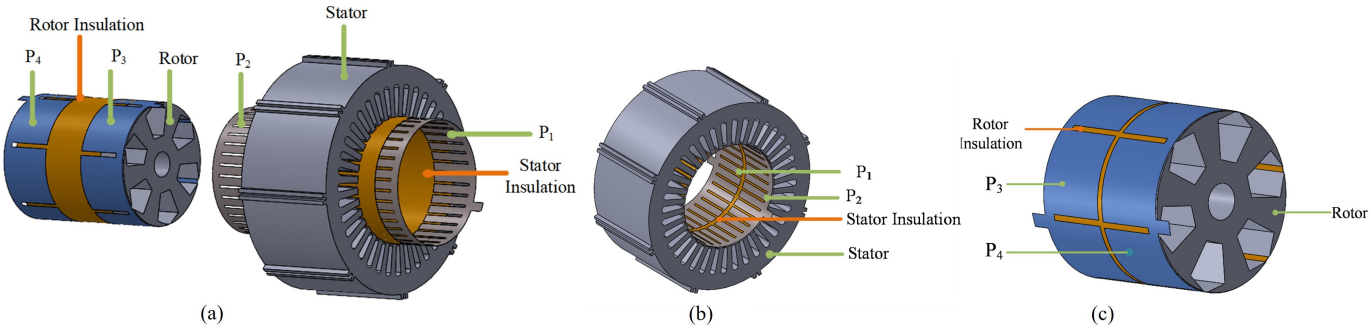

Fig. 1. 3D model of the proposed design. (a) Exploded view of the proposed design. (b) Stator plates on the rotor core. (c) Rotor plates on the rotor core.

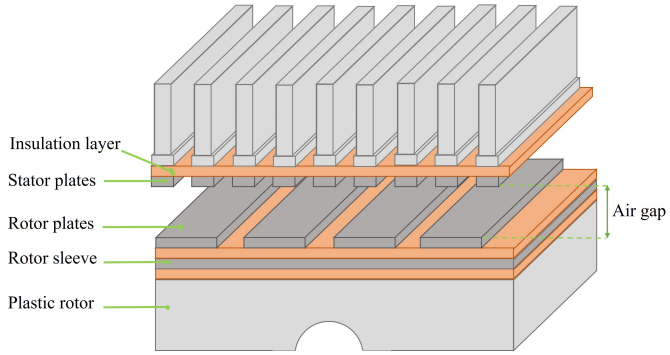

Fig. 2. Flat cross-sectional view of the proposed prototype.

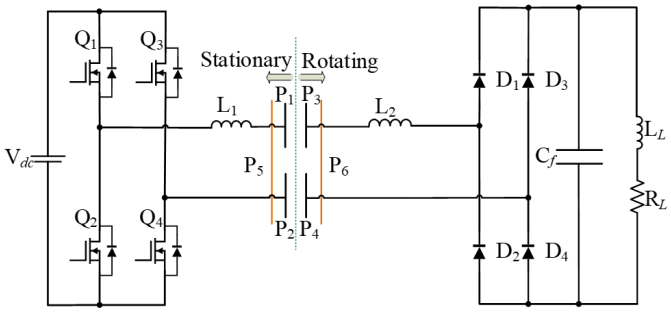

Fig. 3. Circuit diagram of the proposed CPT system.

this paper is mounting the plates inside the machine air gap on the stator and rotor core. The capacitive plates are cut into strips and joined together through a circular ring. The shape is chosen to minimize undesired impact on the machine's torque so the strips replicate the stator teeth and the rotor pole length. Eventually, a cylindrical rotary coupler is formed [13].

In Fig. 1(b), P_1 and P_2 represent the transmitter plates placed on the stator's inner surface with insulation. In Fig. 1(c), P_3 and P_4 represent receiving plates placed on the rotor outer surface with insulation. Selected insulation material has been placed between the plates and cores for electrical isolation. Fig. 2 represents the flat cross-sectional view of the developed machine prototype. An additional metal sheet is applied over a plastic rotor to simulate the capacitance coupling present in a real rotor. The stator and the rotor core proximity establishes the rotor and stator plate P_5 and P_6. Fig. 3 represents the circuit diagram of the proposed CPT system.

The input voltage V_{dc} and the full bridge inverter are modeled as a high-frequency AC voltage source. The field winding impedance represented by R_L and L_L along with a full bridge rectifier is modeled as an equivalent AC resistance. L_1 and L_2 inductors represent the primary and secondary compensation elements and are evaluated using the resonant relationship presented in (1) and (2), respectively.

$$L_1 = \frac{1}{\omega_s^2 C_{pri}} \tag{1}$$

$$L_2 = \frac{1}{\omega_s^2 C_{sec}} \tag{2}$$

In (1) and (2), ω_s is the radial switching frequency, and C_{pri} and C_{sec} are the capacitances of the coupler system referred to primary side and secondary side, respectively [11]. The CPT system operating frequency is in the MHz range, and the armature current frequency is typically below a few 100's Hz. Hence, the two systems do not interfere with each other.

III. WFSM Electromagnetic Design

The CPT system has been designed following the characteristic of an existing machine whose dimensions are tabulated in Table I. The motor considered for the development and

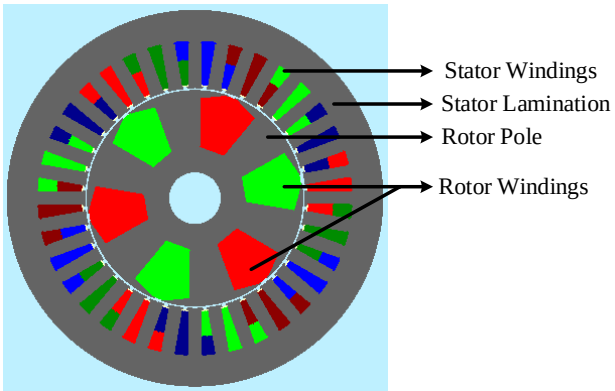

Fig. 4. 2D schematic of the investigated motor.

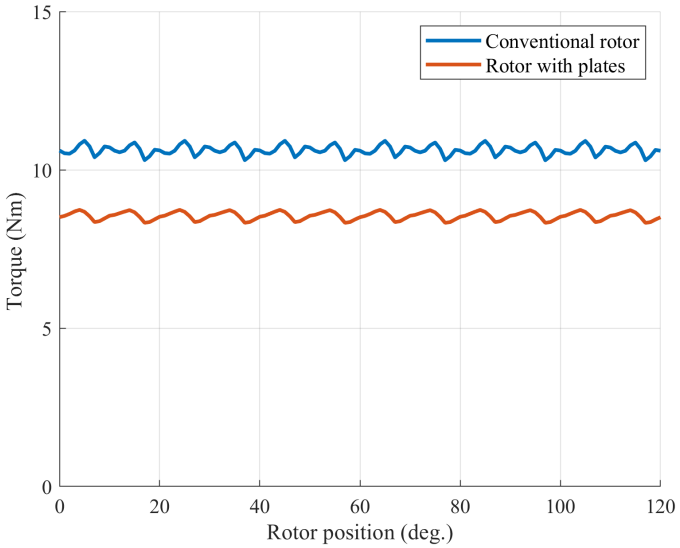

Fig. 5. Torque profile of the studied WFSM obtained from FEA simulations.

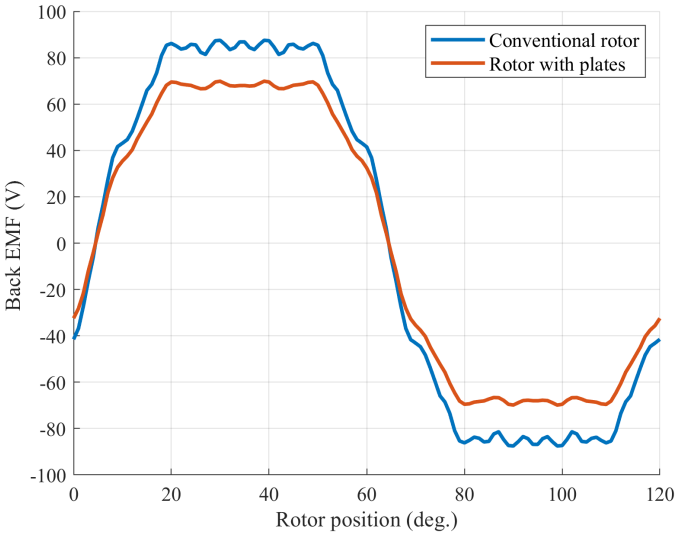

Fig. 6. Back EMF waveforms of WFSM obtained from FEA simulations.

TABLE I
MOTOR PARAMETERS

Parameter	Value
Stator OD	180 mm
Rotor OD	98 mm
Air Gap	0.8 mm
Stack Length	85 mm

verification of the integrated CPT approach is a 36 slot/6 pole WFSM, although the proposed strategy is equally applicable to WFSMs of all slot/pole topology. As seen in Fig. 4, the stator windings are short pitched by one slot to minimize the torque ripple. The design is carried out using 2D electromagnetic FEA.

FEA simulation was also used to observe the effect of current in the CPT plates on the motor torque, and there was no observable effect of CPT operation on the motor air gap flux density and torque. The torque ripple waveforms obtained from FEA simulations are shown in Fig. 5. Although the CPT plates are made of electrical steel and do not contribute to the main flux path reluctance, the insulation between the plates and motor lamination are non-magnetic, which increases the effective air gap of the motor. This results in a drop in the output torque. However, the back EMF is also proportionally reduced, as seen in Fig. 6, and as a result, the motor with integrated CPT plates can achieve higher speeds for the same supply voltage, and the maximum output power remains approximately constant as in the conventional rotor WFSM, despite the drop in peak torque. A trade-off between efficiency and torques based on the machine design is described in the next section.

IV. COUPLER DESIGN OPTIMIZATION

The geometric parameters of the capacitive plates influence the efficiency and torques of the system. The rotating stator magnetic field and the high frequency current flowing in a

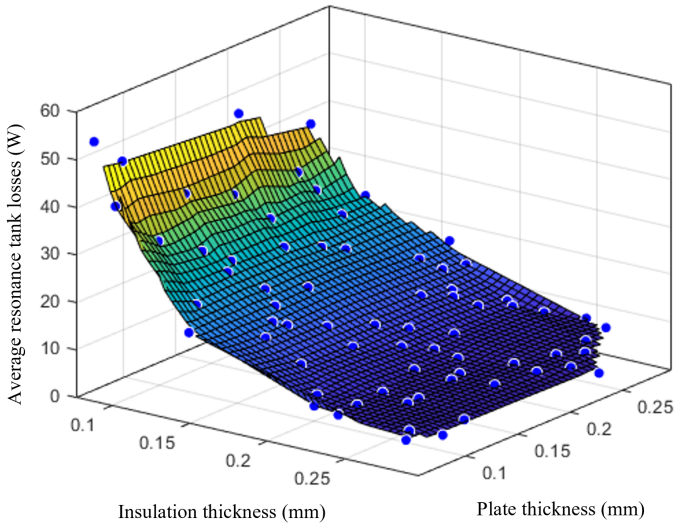

Fig. 7. Resonance tank losses.

CPT system should be included in the losses evaluation. As the capacitive plates are not laminated, eddy currents due to stator magnetic field can not be neglected. Furthermore, the high frequency current flowing in the CPT system generates resistive losses in the capacitive plates and the matching network components. This latter may represent a significant source of loss for a specific design. Fig. 7 shows the average resonant tank losses related to the insulation and plate thickness. While the effect of the plate thickness is practically negligible, the insulation layer has a significant impact, especially in designs where the parameter is smaller than 0.15 mm. Designs with smaller insulation thickness have a higher cross-coupling capacitance effect between the plates and the stator and rotor core. Consequently, due to the parasitic effect, a higher amount of current is required to achieve the same output power, causing the resistive loss of the circuit components to increase.

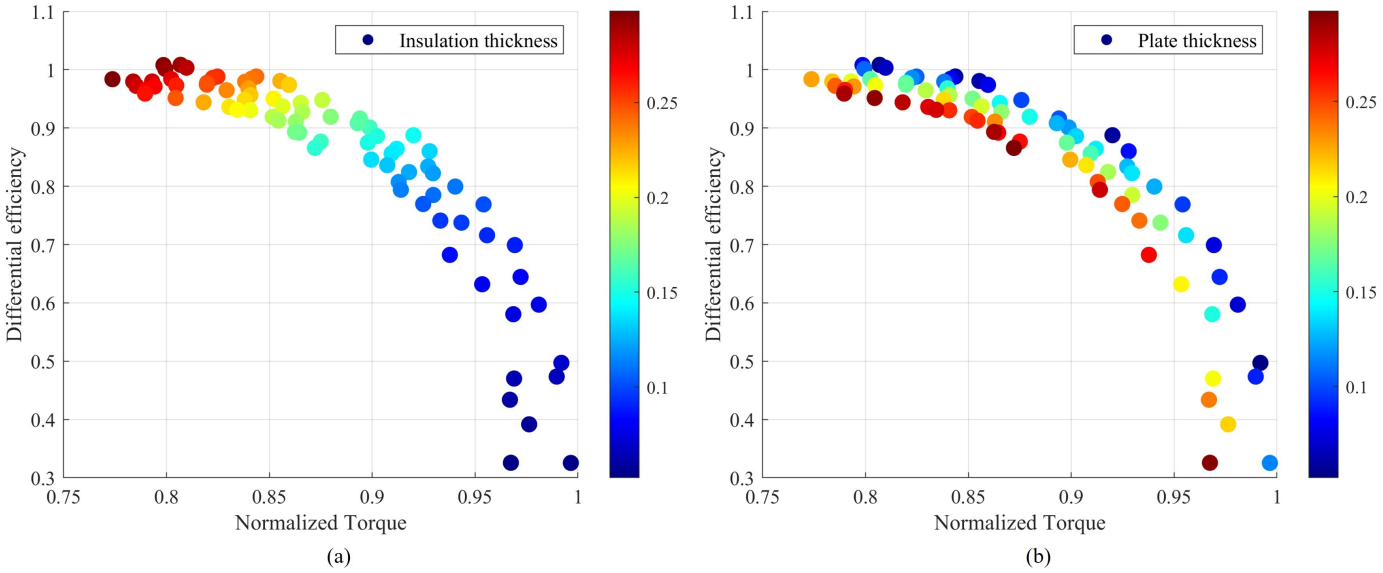

Fig. 8. Pareto front in the dual-objective optimization with efficiency and torque as objective functions: (a) insulation thickness (b) plate thickness.

Normalized torque and normalized system efficiency have been selected as performance parameters of the proposed coupling structure. The output torque of the proposed machine design is normalized with the torque in a conventional WFSM with the same gap i.e. 0.8 mm. The same has been done with the efficiency of the proposed design and the efficiency of an equivalent slip-ring based system in a conventional WFSM. A differential efficiency η_Δ has been used as a parameter to estimate the performance of the CPT system. These parameters are evaluated in (3) and (4). The Δ_{loss} is the difference between the losses present in the machine with a CPT system and the losses present in a conventional slip-ring based machine. The core and copper losses of the machine are included in the analysis. $P_{loss,CPT}$ includes the losses in the CPT system. The considered CPT system losses include the losses in the compensation circuit and rectifier. $P_{loss,conv}$ refers to the conventional WFSM losses that consist of machine core losses and the losses in the brushes $P_{loss,brushes}$.

The losses of the proposed design are compared with the losses of the conventional machine with carbon brushes [12]. The voltage drop losses in the conventional machine across the brush-slip ring assembly is ≈ 5.3 W, evaluated from (5). Here, V_{drop}, the voltage drop between the brushes and the rotating side,is taken 2.3 V, R is brushes resistance, estimated to 19 $m\Omega$ and I_{field} of 2.3 A is the field winding rated current.

$$\eta_\Delta = \frac{P_{out}}{P_{out} + \Delta_{loss}} \tag{3}$$

$$\Delta_{loss} = P_{loss,CPT} - P_{loss,conv} \tag{4}$$

$$P_{loss,brushes} = RI_{field}^2 + V_{drop} I_{field} \tag{5}$$

Table II provides coupler design parameters that have been varied to analyze the performance parameters. For simplicity, D_{Ri} is taken equal to D_{Si} and similarly for D_{Rp} and D_{Sp}. A Pareto front obtained after varying the insulation and plate thickness of the design is shown in Fig. 8. Fig. 8(a) provides the Pareto obtained by varying the insulation thickness. Higher values of the insulation thickness provide less torque but more efficiency, and vice versa. Fig. 8(b) shows the Pareto front for the variation of the plate thickness. The thinner the plate, the higher the system efficiency and machine torque.

TABLE II
PLATE PARAMETERS DESCRIBING THE STRUCTURE

Description	Parameter	Description	Parameter
Rotor Insulation Thickness	D_{Ri}	Rotor Plate Thickness	D_{Rp}
Stator Insulation Thickness	D_{Si}	Stator Plate Thickness	D_{Sp}

As can be noticed, some of the designs show a differential efficiency greater than 1. Considering (4), this indicates that the losses in the conventional machine are higher than the one present in the proposed CPT based system, ending up with a system with better efficiency.

V. PROTOTYPE DEVELOPMENT AND EXPERIMENTAL RESULTS

In this section, the prototyping development process is described. Moreover, experimental tests are presented to support the analysis. A 36-slots 4-pole stator core is employed for mounting the stator power transfer plates, as shown in Fig. 9(c). In Fig. 9(a), a CNC machined rotor is made from High-Density Polyethylene (HDPE) material. The rotor replica is housed inside an electrical steel sleeve to simulate the capacitive plate P_6 of the rotor core. Fig. 9(b) presents the rotor receiving plates P_3 and P_4. Fig. 9(c) shows the placement of transmitter plates P_1 and P_2 on the stator. The rotor plates and the stator plates are held in position with an insulation layer of Kapton tape. This provides electrical isolation between

TABLE III
PROTOTYPE AND CIRCUIT PARAMETERS

Parameter (mm)	Stator Inner Radius	Stack Length	Rotor Outer Radius	Plate Thickness	Insulation Layer Thickness
Value	50	85.5	48.3	0.127	0.2
Parameter	C_{1eqpi} (pF)	C_{2eqpi} (pF)	C_m (pF)	L_1 (μH)	L_2 (μH)
Measured Value	437	838	152.6	14.5	7.85

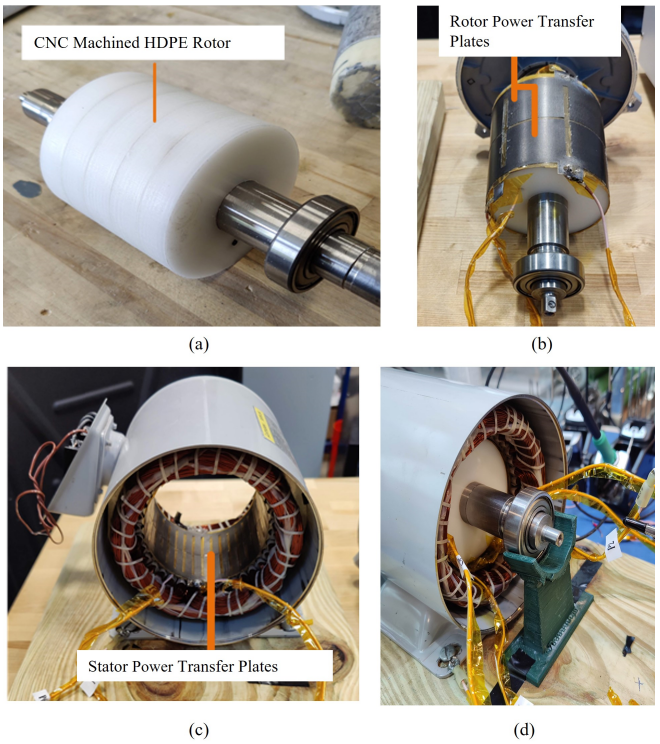

Fig. 9. Prototype development (a) Development of the rotor replica. (b) Rotor plates mounted on the rotor. (c) Stator plates mounted on the stator. (d) Complete assembly of the prototype.

the capacitive plates and the machine core. Litz wire of adequate length has been soldered with all six plates of the coupler structure to measure the inter-plate capacitance. A complete assembly of the prototype is shown in Fig. 9(d). The impact of insulation and plate thickness on the performance parameters is the criteria for selecting the thickness of the insulation and plate material. However, market accessibility for specific thicknesses has been considered when developing the prototype.

Fig. 10 shows the experimental setup for the power test. A double sided LL compensation network has been used. The parameters of the prototype, the measured values of the equivalent 2-port capacitance model, and resonant inductors are tabulated in Table III. A linear power amplifier and an antenna tuner are used as a sinusoidal source voltage, and an equivalent AC resistance of 15Ω is used as load. Air core inductors L_1 and L_2 are connected to the transmitting and receiving sides of the system. The test is performed up to 64 W of load power. The oscilloscope waveform in Fig. 11

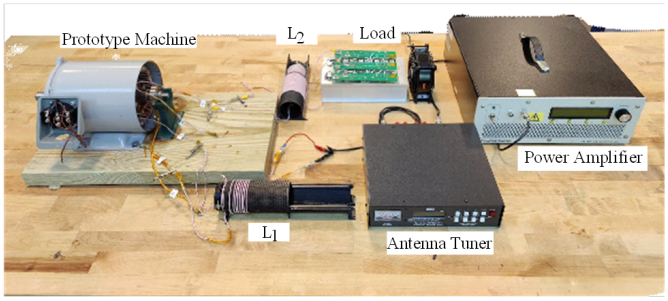

Fig. 10. Experimental setup for power testing.

shows the load current I_{load} of 2.065 A, the plate voltage V_{13} of 237.5 V, and V_{56} of 26.71 V at 64 W power transfer. In Fig. 12, it can be seen that the source voltage V_s is 32.55 V, the source current I_s is 2.75 A, and the plate voltage V_{12} is 480 V.

Fig. 13 compares simulation and experimental values of the system performance. Fig. 13(a) shows a good agreement between the measured and simulated value of the voltage V_{13} between power transfer plates P1 and P3. An alternative way to evaluate the electric field emission in the surrounding environment is the measurement of voltage V_{56} across P5 and P6 plates. The lower the V_{56} voltage the lower will be electric field emission in the surrounding environment [11]. Fig. 13(b) shows that V_{56} voltage simulated is lower than experimental values. This could be due to the imperfections in physical design of couplers and it can be improved with advanced manufacturing techniques. The maximum V_{56} voltage is 27 V at rated power and the corresponding electric field reduces to IEEE electric field emission limit of 110 V/m at 0.2 mm of distance from the stator core. This value complies with the electric field emission standard [14].

It is worth mentioning that there is a significant research gap in evaluating power losses in the coupler plates. Generally, the researchers do not consider the losses in the plates or assign all the unknown losses in the system as plate losses [11], [15]. However, the significant difference between experimental and simulation based efficiency has motivated the authors to investigate the losses in the coupler plates. A first set of results demonstrated a 10% difference between the simulated and experimental efficiency. After that, the capacitive plate losses are reevaluated using ANSYS High Frequency Simulation Software (HFSS). The HFSS has been employed for evaluating the losses in the plates. A Z parameter was obtained from the simulation at 2 MHz by utilizing the Lumped Port Excitation

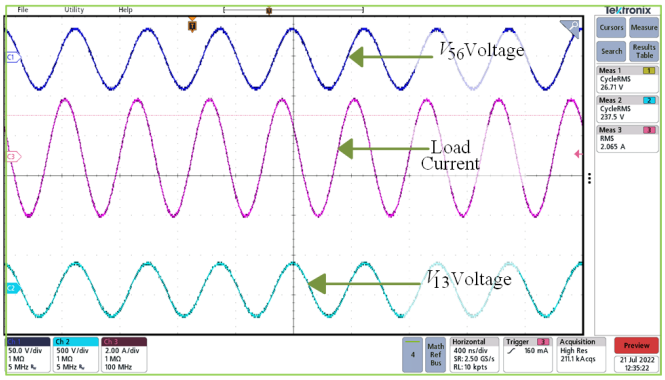

Fig. 11. Oscilloscope waveforms V_{56}, I_L and V_{13}.

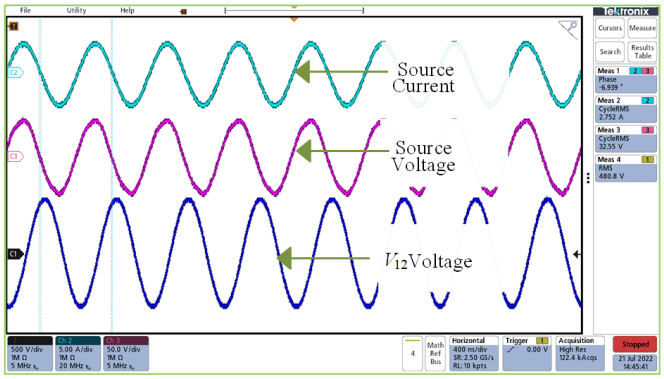

Fig. 12. Oscilloscope waveforms V_{12}, I_s, and V_s.

between the two plate terminals. That led to including not only electric, but also magnetic field in the simulation which provided more realistic loss estimation. Consequently, the losses within the plates have been accounted for properly. Fig. 13(c) shows the efficiency of the proposed CPT system. The simulated value of efficiency is approximately constant. The experimental efficiency shows good correlation with the simulated efficiency. Further evaluation of the proposed CPT system in a practical environment, including the rotor spinning while being powered by the CPT system, is part of the ongoing research and will be presented in some future publications.

VI. Conclusion

A novel design of CPT for rotor excitation in a WFSM has been proposed. The proposed coupler design has been installed in the machine's air gap. Thus, it can improve the volumetric power density compared to the previous design. A 64 W power has been transmitted with 81.3% coupler efficiency at 2 MHz operating frequency. The proposed design has been prototyped and experimentally tested. The proposed CPT system will be verified with a machine in running condition.

References

[1] E. Sokolov, "Comparative study of electric car traction motors," *2017 15th International Conference On Electrical Machines, Drives And Power Systems (ELMA)*. pp. 348-353 (2017)

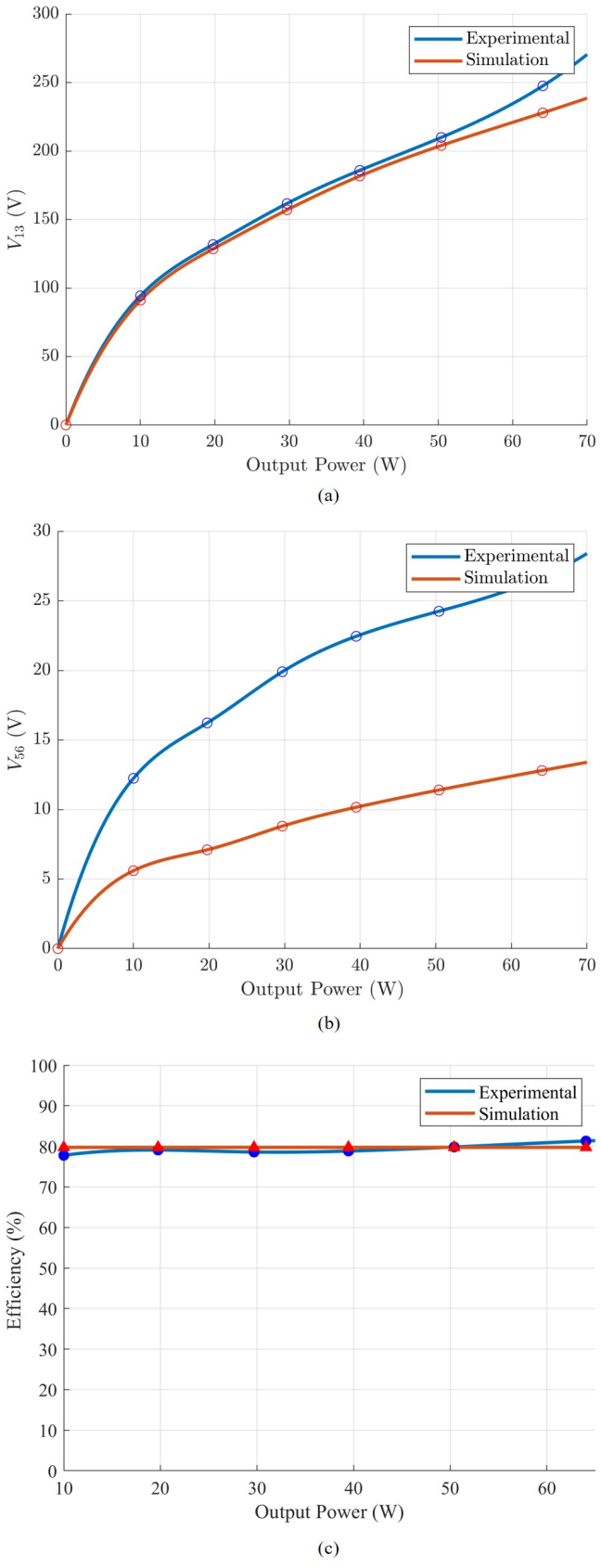

Fig. 13. (a) V_{13}, (b) V_{56}, and (c) Efficiency comparison between experimental and simulation results.

[2] Z. Wang, T. Ching, S. Huang, H. Wang, and T. Xu, "Challenges Faced by Electric Vehicle Motors and Their Solutions," *IEEE Access*. vol. 9 pp. 5228-5249 (2021)

[3] J. Nøland, S. Nuzzo, A. Tessarolo, and E. Alves, "Excitation System Technologies for Wound-Field Synchronous Machines: Survey of Solutions and Evolving Trends". *IEEE Access*. vol. 7 pp. 109699-109718 (2019)

[4] M. Erel, K. Bayindir, M. Aydemir, S. Chaudhary, and J. Guerrero, "A Comprehensive Review on Wireless Capacitive Power Transfer Technology: Fundamentals and Applications," *IEEE Access*. vol. 10 pp. 3116-3143 (2022)

[5] J. Liu, and T. Lipo, "Synchronous machine field excitation utilizing a single phase matrix converter excited rotary transformer," *2017 IEEE Energy Conversion Congress And Exposition (ECCE)*. pp. 1197-1204 (2017)

[6] C. Stancu, T. Ward, K. Rahman, R. Dawsey, and P. Savagian, "Separately Excited Synchronous Motor With Rotary Transformer for Hybrid Vehicle Application," *IEEE Transactions On Industry Applications*. vol. 54, 223-232 (2018)

[7] D. Ludois, K. Frankforter, B. Ge, A. Ghule, P. Killeen, and R. Knippel, "Macroscale Electrostatic Rotating Machines and Drives: A Review and Multiplicative Gain Performance Strategy," *IEEE Journal Of Emerging And Selected Topics In Power Electronics*. vol. 10, 14-34 (2022)

[8] D. Ludois, M. Erickson, and J. Reed, "Aerodynamic Fluid Bearings for Translational and Rotating Capacitors in Noncontact Capacitive Power Transfer Systems," *IEEE Transactions On Industry Applications*. vol. 50, 1025-1033 (2014)

[9] J. Dai, and D. Ludois, "A Survey of Wireless Power Transfer and a Critical Comparison of Inductive and Capacitive Coupling for Small Gap Applications," *IEEE Transactions On Power Electronics*. vol. 30, 6017-6029 (2015)

[10] S. Hagen, J. Dai, I. Brown, and D. Ludois, "Low-Cost, Printed Circuit Board Construction, Capacitively Coupled Excitation System for Wound Field Synchronous Machines," *2019 IEEE Energy Conversion Congress And Exposition (ECCE)*. pp. 5358-5364 (2019)

[11] H. Zhang, F. Lu, H. Hofmann, W. Liu, and C. Mi, "Six-Plate Capacitive Coupler to Reduce Electric Field Emission in Large Air-Gap Capacitive Power Transfer," *IEEE Transactions On Power Electronics*. vol. **33**, 665-675 (2018)

[12] Mersen Company. *Mersen Carbon brushes for motors and generators*, 2010.

[13] Liu, C., Hu, A. & Nair, N. "Coupling study of a rotary Capacitive Power Transfer system." *2009 IEEE International Conference On Industrial Technology*. pp. 1-6 (2009)

[14] "IEEE Standard for Safety Levels with Respect to Human Exposure to Radio Frequency Electromagnetic Fields, 3 kHz to 300 GHz," in *IEEE Std C95.1, 1999 Edition* , vol., no., pp.1-83, 16 April 1999

[15] B. Regensburger, A. Kumar, S. Sinha, K. Doubleday, S. Pervaiz, Z. Popovic, and K. Afridi, "High-performance large air-gap capacitive wireless power transfer system for electric vehicle charging," *2017 IEEE Transportation Electrification Conference And Expo (ITEC)*. pp. 638-643 (2017)